Available online at www.sciencedirect.com
ScienceDirect
Polymer 48 (2007) 6668–6680
polymer
www.elsevier.com/locate/polymer

Acceleration or retardation to crystallization if liquid–liquid phase separation occurs: Studies on a polyolefin blend by SAXS/WAXD, DSC and TEM

Yanhua Niu [a], Zhigang Wang [a,*], Carlos Avila Orta [b], Donghua Xu [a], Howard Wang [c], Katsumi Shimizu [d], Benjamin S. Hsiao [e], Charles C. Han [a]

[a] *CAS Key Laboratory of Engineering Plastics, Joint Laboratory of Polymer Science and Materials, Beijing National Laboratory for Molecular Sciences, Institute of Chemistry, Chinese Academy of Sciences, Beijing 100080, PR China*
[b] *Centro de Investigación en Química Aplicada. Blvd. Enrique Reyna H. No. 140. Saltillo, Coahuila, C.P. 25253, México*
[c] *Department of Mechanical Engineering, State University of New York at Binghamton, Binghamton, New York 13902, USA*
[d] *Advanced Protein Crystallography Research Group, RIKEN Harima Institute, 1-1-1 Kouto, Sayo-chou, Sayo-gun, Hyogo 679-5148, Japan*
[e] *Department of Chemistry, Stony Brook University, Stony Brook, NY 11794, USA*

Received 15 June 2007; received in revised form 14 August 2007; accepted 22 August 2007
Available online 1 September 2007

Abstract

Blends of statistical copolymers containing ethylene/hexene (PEH) and ethylene/butene (PEB) exhibited the behavior of upper critical solution temperature (UCST). The interplay between the early and intermediate stage liquid–liquid phase separation (LLPS) and crystallization of the PEH/PEB 50/50 blend was studied by time-resolved simultaneous small-angle X-ray scattering (SAXS) and wide-angle X-ray diffraction (WAXD) techniques. Samples were treated by two different quench procedures: in single quench, the sample was directly quenched from 160 °C to isothermal crystallization temperature of 114 °C; while in double quench, the sample was firstly quenched to 130 °C for 20 min annealing, where LLPS occurred, and then to 114 °C. It was found that in the early stage of crystallization, the integrated values of Iq^2 and crystallinity, X_c, in the double quench procedure were consistently higher than those in the single quench procedure, which could be attributed to accelerated nucleation induced by enhanced concentration fluctuations and interfacial tension. In the late stage of crystallization, some morphological parameters were found to crossover and then reverse, which could be explained by retardation of lamellar growth due to phase separation formed during the double quench procedure. This phenomenon was also confirmed by DSC measurements in blends of different compositions at varying isothermal crystallization temperatures. The crystal lamellar thickness determined by SAXS showed a good agreement with TEM observation. Results indicated that the early stage LLPS in the PEH/PEB blend prior to crystallization indeed dictated the resulting lamellar structures, including the average size of lamellar stack and the stack distribution. There seemed to be little variation of lamellar thickness and long period between the two quenching procedures (i.e., single quench versus double quench).

Keywords: Crystallization; Liquid–liquid phase separation; Polyolefin blend

1. Introduction

Miscibility in polyolefin blends has long been an interesting subject because the constituting components have similar chemical structures and close refractive indices, making it very difficult to detect the signs of liquid–liquid phase separation (LLPS) in the molten state [1]. For polyethylene blends, there have been notable discrepancies between different measurements and different researchers on this subject. For example, Hill et al. [2,3] reported that LLPS is a ubiquitous phenomenon in blends containing linear and lightly branched polyethylene. Wignall et al. [4,5] presented their small-angle

* Corresponding author. Tel./fax: +86 10 62558172.
E-mail address: zgwang@iccas.ac.cn (Z. Wang).

0032-3861/$ - see front matter © 2007 Elsevier Ltd. All rights reserved.
doi:10.1016/j.polymer.2007.08.060

neutron scattering (SANS) results of mixtures containing linear polyethylene and ethylene copolymers, and they concluded that the occurrence of LLPS depends on the branch content of ethylene copolymers. They opposed the argument by Hill et al. [2] that the blend morphology in the solid state cannot appropriately represent that in the molten state because liquid–solid phase separation may take place. Nevertheless, the broad distribution of comonomer content in the branched polyethylene that Hill et al. used might readily result in phase separation. A review by Crist and Hill [1] suggested that besides the inherent isotope effect in the SANS study, the low spatial resolution of SANS might also make the techniques insensitive to large-scale phase separation. Crist and Nesarikar [6] also investigated the late-stage coarsening of polyethylene copolymer blends, considering both coalescence and Ostwald ripening processes. Recently, our group reported the upper critical solution temperature (UCST) phase diagram for nearly isorefractive blends of statistically random ethylene/hexene (PEH) and ethylene/butene (PEB) copolymers by using small-angle light scattering technique [7], where results clearly indicated the interplay between LLPS and crystallization. This phase diagram was further confirmed by rheological measurements [8], where viscoelastic responses gave the direct evidence of LLPS for metallocene-based polyethylene blends containing different branch contents.

Although a great deal of literatures dealing separately with LLPS and crystallization behaviors for polyolefin blends from both theoretical and experimental aspects have been presented, there have been relatively limited publications treating the occurrence of LLPS and crystallization simultaneously [9–11]. This is because the interactions between these two non-equilibrium phase transition processes (i.e., LLPS and crystallization), which are dominated by thermodynamics and kinetics driving forces, respectively, can be quite complicated. Hashimoto et al. [9,10] systematically studied the morphological evolution in polyolefin blends containing polypropylene (PP) and ethylene–propylene rubber (EPR) by carefully controlling the LLPS and crystallization conditions. They found that the readily formed modulated structure could be ''locked in'' during crystallization as long as the crystallization rate was relatively rapid. In the study of partially miscible blends of isotactic polypropylene (*i*-PP) and isotactic poly(1-butene) (*i*-P_1B) [11], Cham et al. observed that spherulites of *i*-PP could take place continuously from the readily formed *i*-PP-rich phase to the *i*-P_1B-rich phase, but the growth rate in the former was relatively faster than that in the latter depending on crystallization temperature.

Our group has reported a series of publications [12–18] dealing with the competition between LLPS and crystallization for the aforementioned PEH/PEB blends. We showed that in a simultaneously crystallizing and phase separating polymer blend, the morphology development exhibited a ''crossover'' feature [12,13] (at 118 °C for the PEH/PEB 50/50 blend) from dominated crystal lamellar morphology to dominated liquid phase-coarsening morphology. This crossover behavior is ubiquitous for blends with the critical temperature of LLPS above the equilibrium melting temperature of the crystalline component [7] and can be explained by the different quenching processes. In an intermediate temperature range close to the crossover, the competition between LLPS and crystallization would result in the suppression of crystal growth rate near the critical composition. We have compared the time evolution of morphological parameters during one-step crystallization of the PEH/PEB 50/50 blend and pure PEH at various crystallization temperatures [14]. It was found that the temperature dependence of these parameters for the PEH/PEB 50/50 blend could be explained by the competition between LLPS and crystallization with respect to the crossover temperature. All experimental results seem to support the mechanism of ''fluctuations-assisted crystallization'' [15,16], where the spontaneous fluctuations of LLPS can overcome the nucleation barrier and assist the process of crystallization, which, in other system, such as polycarbonate/poly(ethylene oxide) (PC/PEO) blends was also found by Tsuburaya and Saito [19]. According to the report of Madbouly and Ougizawa [20], the major acceleration in the crystallization kinetics was observed for poly(ε-caprolactone)/poly(styrene-*co*-acrylonitrile) (PCL/SAN) blend, which underwent early and intermediate stage phase separation. In a recent publication for PEH/PEB system [17], we observed a fine dot-like structure inside the phase domains when the sample was quenched from phase separation temperature to room temperature (this was regarded as crystallization-induced phase separation). Our results also indicated that the lamellar long period of the PEH/PEB blend near the critical composition exhibited a minimum value, which was a function of LLPS temperature, LLPS time and crystallization temperature [18]. This complex phenomenon was explained by the simultaneously occurring exclusion/inclusion of the amorphous component, crystal lamellar insertion and lamellar thickening processes.

Although the interplay between LLPS and crystallization for the chosen PEH/PEB blend has been understood to a large extent, our previous works dealt mainly with the behavior of the relatively late stages of phase separation. At these stages, the concentration fluctuations were nearly saturated and the coarsening of microphase domains occurred primarily by self-similarity. It is conceivable that at the earlier stages of LLPS, the situation might be quite different, whereby the interplay between LLPS and crystallization may play a more dominant role than those in our previous studies. For this purpose, we have investigated the effects of early and intermediate stages of LLPS on the crystallization behavior by using simultaneous synchrotron time-resolved small-angle X-ray scattering (SAXS) and wide-angle X-ray diffraction (WAXD) techniques and DSC measurements. The time evolution of structural and morphological variables, including the scattering invariant, crystallinity, lamellar long periods of the PEH/PEB 50/50 blend during isothermal crystallization at 114 °C was followed by real time X-ray techniques using one-step quench (single quench) or two-step quench (double quench) procedures from the homogenous melt. DSC results on the PEH/PEB 50/50 blend, pure PEH and the PEH/PEB 70/30 blend at isothermal crystallization temperature of 114 °C and on the PEH/PEB 50/50 blend at 116 °C in single and double

quench procedures, respectively, were also performed to provide complementary information. Based on experimental results from in situ X-ray/thermal studies and ex situ TEM observations, several new insights into the interplay between the earlier stages of LLPS and crystallization for the PEH/PEB blends have been obtained.

2. Experimental

2.1. Materials and sample preparation

Polymers used in this study included PEH, a statistical copolymer of ethylene and hexene ($M_w = 112{,}000$ g/mol, $M_w/M_n \sim 2$, and branch density of 9 CH_3 per 1000 backbone carbon), and PEB, a statistical copolymer of ethylene and 1-butene ($M_w = 70{,}000$ g/mol, $M_w/M_n \sim 2$, and branch density of 77 CH_3 per 1000 backbone carbon). These polymers were kindly supplied by ExxonMobil Chemical Company. They were synthesized by using metallocene catalysts and possessed the same structures as those used in our previous studies [7,8,12–18]. The dried solution-precipitated PEH and PEB samples exhibited T_m of 119.8 °C and 48.6 °C, respectively, by using DSC scans at a heating rate of 10 °C/min. In this study, the PEH/PEB 50/50 blend was prepared by coprecipitating the mixture from a hot xylene solution (about 100 °C) into cold methanol (about 0 °C). After filtering, the recovered floccule was firstly air-dried for 24 h and then vacuum-dried at 60 °C for 72 h until the solvent was completely removed. The dried floccule was molded into void-free disks with 7 mm in diameter and 1.5 mm in thickness for X-ray scattering and diffraction measurements. In addition, the PEH/PEB 70/30 blend and pure PEH were also prepared by following the same procedure for DSC measurements.

The measured and calculated phase diagram for the PEH/PEB blends [7] is illustrated in Fig. 1. This phase diagram contains an upper critical solution temperature (UCST) with critical temperature $T_{cri} = 146$ °C and critical composition ϕ_{cri} (mass fraction) = 0.44, as well as the calculated binodal and spinodal boundary lines (shown as solid and dashed lines, respectively). The open square represents the measured equilibrium melting temperature, T_m^o [7]. A similar UCST phase behavior has also been observed in blends of other branched polyolefins [21,22]. The value of T_m^o for PEH is about 140 °C, much higher than that of PEB. Thus, at the crystallization temperature in this study ($T_c = 114$ or 116 °C), PEH represents the crystallizable component while PEB represents the amorphous component.

2.2. Time-resolved SAXS/WAXD measurements

Time-resolved simultaneous SAXS/WAXD experiments were performed at the Advanced Polymers Beamline, X27C, in National Synchrotron Light Source (NSLS), Brookhaven National Laboratory (BNL). The wavelength of the X-ray beam was 1.366 Å and the beam size was about 0.4 mm in diameter at the sample position. SAXS/WAXD profiles were recorded by two linear position sensitive detectors (European Molecular Biological Laboratory, EMBL), with the sample-to-detector distances of 1788 mm for SAXS and 220 mm for WAXD. The SAXS scattering angle was calibrated with silver behenate and the intensity was normalized by incident beam fluctuations and calibrated with a LUPOLEN standard. The WAXD pixel resolution and the diffraction intensity were calibrated by comparing the synchrotron data with those taken using a Siemens Hi-Star X-ray diffractometer data (Cu Kα) in $\theta-\theta$ reflection, and were corrected for detector non-linearity and empty beam scattering. The angular scale of the synchrotron WAXD data ($\lambda = 1.366$ Å) was converted to a scale corresponding to $\lambda = 1.542$ Å for presentation and discussion.

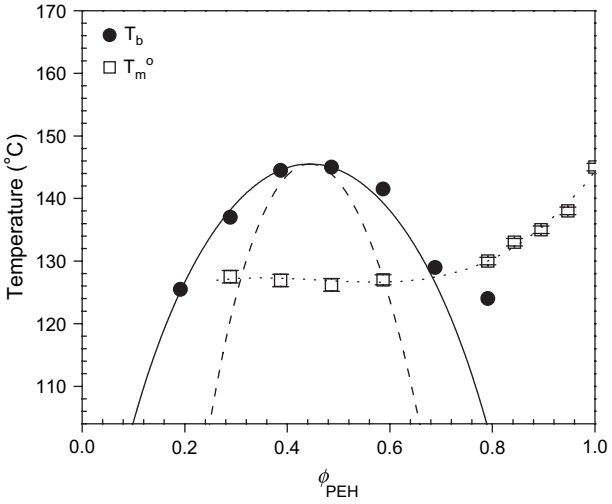

Fig. 1. Phase diagram of the PEH/PEB blends determined by diffusion light scattering method. The symbols are measured data points and the solid and dashed curves indicate the calculated binodal and spinodal boundaries, respectively. The dotted line shows the equilibrium melting temperature, T_m^o. The upper critical solution temperature is at $T_c = 146$ °C and $\phi_c = 0.44$.

A dual chamber temperature jump apparatus was used for the isothermal crystallization study. The detailed description of this setup has been reported elsewhere [23]. In this study, the PEH/PEB 50/50 blend samples were treated with two different procedures: single quench and double quench, respectively. In the single quench procedure, the sample was melted at 160 °C (i.e., 40 °C above the nominal melting point of PEH) for 10 min in the first chamber and then pneumatically "jumped" to the second chamber preheated at a temperature of 114 °C for isothermal crystallization. In the double quench procedure, the sample was melted in the first chamber at 160 °C for 10 min and then rapidly transferred to the second chamber at 130 °C for 20 min, during which the first chamber was also cooled from 160 °C to 114 °C. After annealed at 130 °C for 20 min, the sample was "jumped" back to the first chamber at 114 °C for isothermal crystallization. The actual sample temperature was measured by a calibrated OMEGA J thermocouple, positioned near the sample. At the equilibrated temperature, the maximum temperature fluctuation was ±0.5 °C. The collection time for each simultaneous SAXS/WAXD measurement was 20 s. The temperature profiles for the single quench and double quench procedures are shown in Fig. 2. It is seen that the transition time for from 160 °C

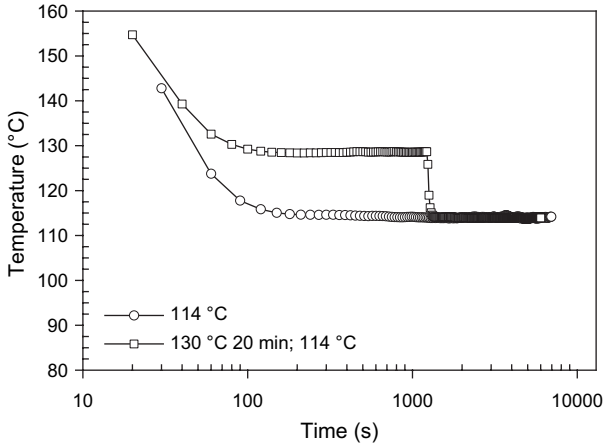

Fig. 2. Time–temperature profiles at the sample position for the single quench and double quench procedures to indicate the precise control of the sample temperature in the experiment.

to 130 °C or 114 °C was about 100 s, and that for from 130 °C to 114 °C was shorter than 100 s.

2.3. DSC measurements

DSC measurements were carried out by using a Perkin–Elmer Diamond DSC instrument with the sample weight of about 4 mg under nitrogen purge. The procedures for the sample treatment were the same as those in the SAXS/WAXD measurements. The samples of the PEH/PEB 50/50, 70/30 blends and pure PEH were firstly heated to 160 °C and held for 10 min to eliminate thermal history. In single quench, samples were directly quenched to 114 or 116 °C for isothermal crystallization. In double quench, samples were firstly quenched to 130 °C and held for 20 min, and then they were subsequently quenched to 114 or 116 °C for isothermal crystallization. The time-resolved exothermal thermograms during isothermal crystallization were recorded.

2.4. TEM observation

Samples for transmission election microscopy (TEM) observation of the PEH/PEB 50/50 blend were directly obtained by microtoming the disk-shape samples after the SAXS/WAXD measurements. The procedure for the TEM sample treatment was as follows. TEM samples were cryogenically cooled (at −30 °C) to produce a deformation-free surface using a glass knife in a cryogenic ultramicrotome (Reichert Ultracut E w/FC4D cryostage). RuO_4 staining solution was prepared by adding 1 ml of NaOCl (10% wt/vol from Aldrich) to 0.02 g $RuCl_3$–nH_2O in a 5 ml vial. The cryogenically microtomed samples were stained in the vapor space above the RuO_4 solution for 7 h, followed by degassing in a hood for several hours. Ultra-thin sections (about 700–750 Å) were prepared at ambient temperature using a diamond knife and water flotation bath. Sections were collected onto 200 mesh carbon-coated formvar grids. TEM images were acquired using the JEOL 2000FX TEM (at 160 kV) and Gatan MSC-794 CCD digital camera.

3. Results and discussion

3.1. Time-resolved SAXS/WAXD results

Fig. 3 shows typical time-resolved (a) Lorentz-corrected SAXS intensity profiles (Iq^2 versus scattering vector q, $q = 4\pi/\lambda \sin\theta$, with 2θ being the scattering angle), and (b) WAXD intensity profiles of the PEH/PEB 50/50 blend, developed during isothermal crystallization at 114 °C in the single quench procedure. During the initial isothermal crystallization period (100 s $\leq t \leq$ 300 s), the SAXS profiles in Fig. 3a indicate a completely disordered structure of the undercooled melt. The scattered intensity profile first exhibits a small maximum at $q \approx 0.0175$ Å^{-1} at 300 s (marked with an asterisk) and then this peak grows rapidly with time until it reaches a plateau value. The occurrence of this initial SAXS peak can be attributed to the formation of lamellar stack structure

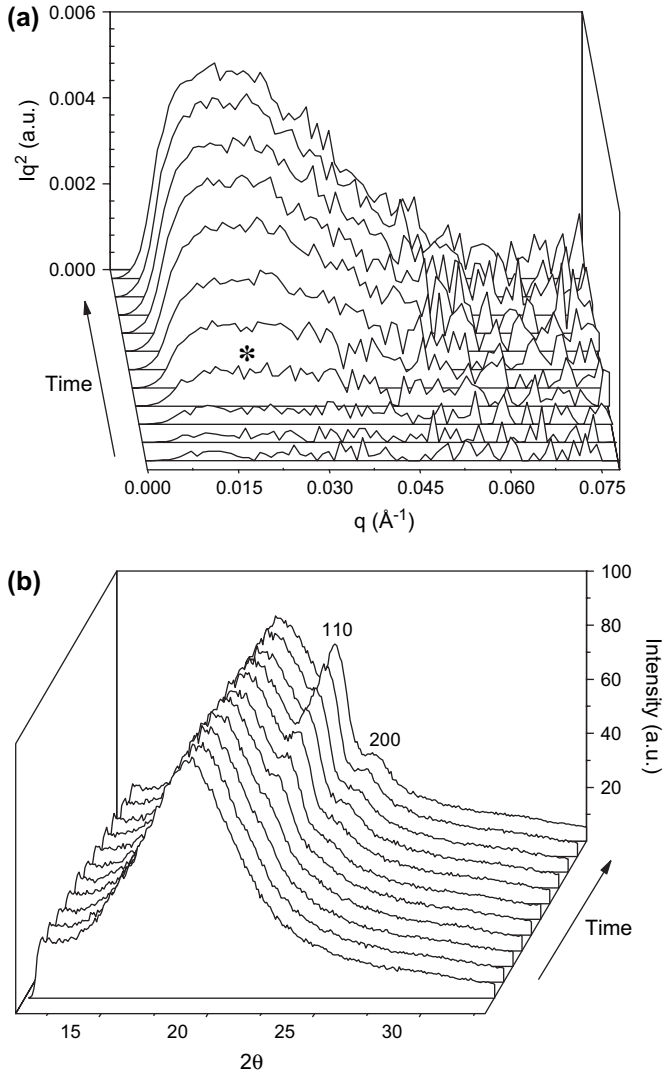

Fig. 3. Typical (a) SAXS and (b) WAXD time-resolved profiles of the PEH/PEB 50/50 blend during isothermal crystallization at 114 °C for the single quench procedure. Time interval between two adjacent profiles is 60 s and the first profile corresponds to 120 s.

in PEH, which is the only crystallizable component at this temperature. In Fig. 3b, the corresponding WAXD profiles in the initial isothermal period only show a diffuse amorphous scattering feature. The evolution of an orthorhombic unit cell from PEH crystals can be followed through the development of the 110 and 200 WAXD reflections. The intensities of these two crystal reflections are found to increase rapidly during the early stage of crystallization and remain almost constant during the late stage of crystallization.

In order to obtain more delicate morphological parameters, such as long period and lamellar thickness, on the basis of SAXS data, quantitative analysis is requisite. For this purpose, real space functions like the one-dimensional correlation function $\gamma_1(r)$ and the interface distribution function $g_1(r)$ are often obtained from experimental data. These real space functions can also be simulated to validate a morphological model. The use of $g_1(r)$ is preferred over $\gamma_1(r)$ since the morphological parameters can be obtained with higher accuracy in the former. According to Santa Cruz et al. [24], the reason for this is that $\gamma_1(r)$ is more affected by the superposition of the maxima or minima of a broad distribution. On the other hand, fitting the simulated function to the experimental one is not an easy task, and in many cases a trial and error fitting process is used. This fitting procedure can be avoided if the reciprocal space data is fitted to a morphological model in reciprocal space, which is much easier to achieve. Later, the simulated pattern in reciprocal space can be transformed into real space to $g_1(r)$ for comparison to the experimental one.

The calculation of $g_1(r)$ requires extrapolating the scattering intensity $I(q)$ to both $q=0$ and $q=\infty$ limits. In the first case, SAXS data was extrapolated to $q\to 0$ using the Debye equation [25]:

$$\underset{q\to 0}{I(q)} = \frac{A}{\left(1+\varepsilon^2 q^2\right)^2} \tag{1}$$

where A is a constant and ε is the length of the inhomogeneity. In the second case, the density profile, as a function of a space vector, r, for an ideal two-phase system resembles a squared-function because the boundaries are assumed to be sharp and the densities within the phases are considered to be constant. As a result, Porod [26] established that the intensity decays proportionally to the inverse of the fourth power of the scattering vector at very large q values, mathematically expressed as

$$\underset{q\to\infty}{I_{\text{ideal}}(q)} = \frac{K_{\text{P}}}{q^4} \tag{2}$$

Eq. (2) is known as the Porod's law, where $I_{\text{ideal}}(q)$ is the scattering intensity of an ideal two-phase system and K_{P} represents the Porod's constant. In fact, $I(q)$ often deviates from the ideality due to the presence of density gradient between the interfaces, and density variations within the phases [27]. The latter often associates with a background scattering intensity, I_{B}, which can produce a positive deviation of the Porod's law; while the former corresponds to a negative deviation related to the interface thickness, E. Assuming a sharp boundary, i.e., $E=0$, Eq. (2) becomes

$$\underset{q\to\infty}{I(q)} = \frac{K_{\text{P}}}{q^4} + I_{\text{B}} \tag{3}$$

If enough data points are taken at large q values, K_{P} and I_{B} can be determined using non-linear least-squares fitting and therefore the ideal scattering intensity, $I_{\text{ideal}}(q)$, can be obtained. However, the selection of q limits requires caution since the choice of both, the lower and upper limits, can significantly affect the validity of the Porod's law. In this study, the upper limit was set to $q_{\text{up}} = 2\ \text{nm}^{-1}$, and the lower limit, q_{low}, was varied until the minimum area of the interference function, $G_1(q)$, was obtained [28], where the interference function is defined as:

$$G_1(q) = K_{\text{P}} - q^4 \cdot I(q) \tag{4}$$

Once the above criterion was achieved, the interface distribution function, $g_1(r)$, can be calculated from the Fourier transform of $G_1(q)$ [29].

$$g_1(r) = \frac{t}{V}\cdot\frac{1}{2\pi^2}\int_0^\infty G_1(q)\cdot\cos(qr)\mathrm{d}q \tag{5}$$

where t is the thickness and V is the volume occupied by the stacking lamellae.

The characteristic distances between the adjacent interfaces, as well as their statistical distributions, can be obtained on the basis of lamellar stacking model [30] having an infinite value at Iq^2.

$$I_{\text{ideal}}(q)\cdot q^2 = \frac{K_{\text{P}}}{q^2}\cdot \text{Re}\left[\frac{H_1\cdot H_2}{1-H_1\cdot H_2}\right] \tag{6}$$

where

$$H_i = 1 - \exp\left[i\cdot l_i\cdot q - \frac{\sigma_i^2\cdot q^2}{2}\right] \tag{7}$$

with l_i being the interface distance between i and $i+1$ and σ_i being the corresponding standard deviation. The interface distances and their distributions can be obtained by means of a non-linear least-squares fitting of $I_{\text{ideal}}(q)\cdot q^2$ values from Eq. (6), in which a weight factor of $1/I_{\text{ideal}}(q)$ was used. It must be kept in mind that the non-linear least-squares fitting was performed on non-smoothed experimental data, corrected by density fluctuations. However, intensity data in the lower and higher q ranges were replaced by data generated by the Debye Eq. (1) and the Porod's law, Eq. (2), respectively. No further smoothing was used. In the lamellar stacking model, two morphological parameters, l_1 and l_2, represent the crystal lamellar thickness and the amorphous layer thickness, respectively. The periodicity or the long period of the lamellar stacks, L, can be estimated as the sum of l_1 and l_2. It should be noted that the correct assignments of l_1 and l_2 as the crystalline lamellar thickness and amorphous layer thickness,

respectively, cannot be accomplished only by the SAXS analysis. Other complementary techniques such as WAXD analysis or TEM observation might be applied to obtain the correct values for the lamellar morphology.

Fig. 4a shows the experimental data and the simulated profile of Lorentz intensity Iq^2 of the PEH/PEB 50/50 blend after 2400 s of crystallization at 114 °C in the single quench procedure. By simulation, the corresponding values of l_1, l_2 and long period, L, were determined. To confirm the validity of the simulated results in Fig. 4a, the related interference function, $G_1(q)$, and the interface distribution function, $g_1(r)$, were simulated by using Eqs. (4) and (5) and compared with the experimental data, which are shown in Fig. 4b and c, respectively. It is seen that the simulated data and the experimental data agree quite well with each other within the ranges of $0 < q < 0.025$ Å^{-1} and $0 < r < 140$ Å. In both cases, outside these ranges the simulated data deviates near the long period region. This effect can be traced back to Fig. 4a, where it is readily seen that the simulated curve can be considered to fit adequately the experimental values although it does not fit perfectly to the $Iq^2(q)$ experimental data. Moreover, since $G_1(q)$ comes from the difference between the ideal value, K_p, and the experimental values, $q^4I(q)$, the deviation increases significantly at higher q values due to fourth power law in q.

For data analysis of WAXD profiles, a peak deconvolution procedure was used. As an example, Fig. 4d summarized the deconvolution results for a WAXD profile collected at 720 s of crystallization in the single quench procedure. The details of this deconvolution procedure have been described elsewhere [31]. In Fig. 4d, the blank circles represent the experimental WAXD data and the solid curve represents the fitted result with a rationally determined baseline illustrated as a dot-dashed line below the profile. The full profile can be considered as a superposition of two crystalline Gaussian peaks (i.e., 110 and 200 crystal reflections), and two amorphous Gaussian peaks as depicted in Fig. 4d. It is noted that two amorphous Gaussian peaks are used for the fitting of the WAXD profiles according to our experience possibly due to the experimental setup. By dividing the total intensity of the two crystal reflections to the overall intensity, the estimated mass fraction of crystal phase in the sample (sometimes referred as the crystallinity index, hereafter termed crystallinity), X_c, can be obtained.

Fig. 5a shows variations of the integrated Iq^2 from SAXS data of the PEH/PEB 50/50 blend with time in the single

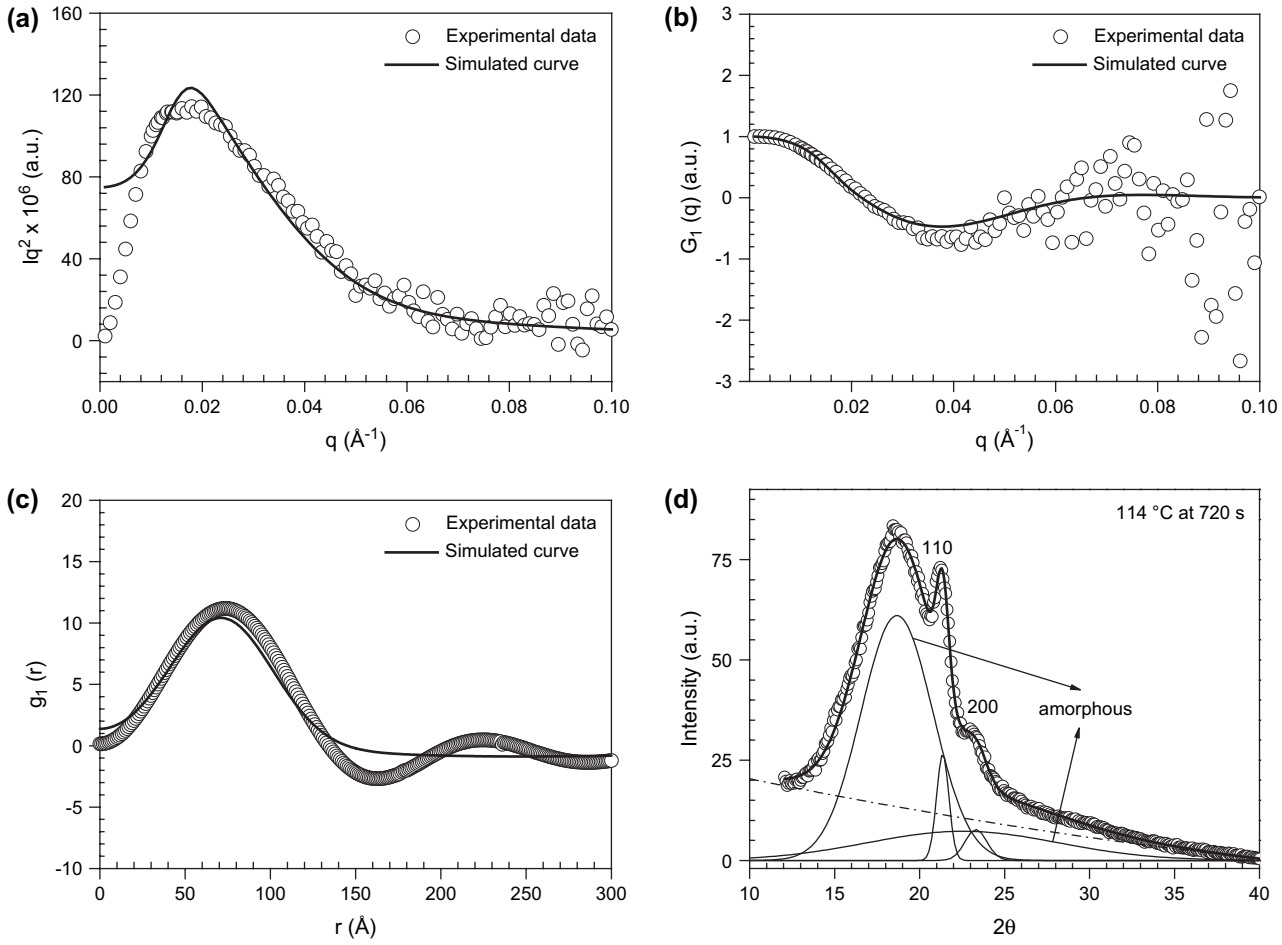

Fig. 4. SAXS data and the simulated profiles of the PEH/PEB 50/50 blend after 2400 s crystallization at 114 °C for the single quench procedure: (a) Lorentz intensity, Iq^2, with wave-vector, q; (b) related interference function $G_1(q)$ with q; (c) interface distribution function, $g_1(r)$, with r; (d) deconvolution result of the WAXD profile of the PEH/PEB 50/50 blend after 720 s crystallization at 114 °C for the single quench procedure.

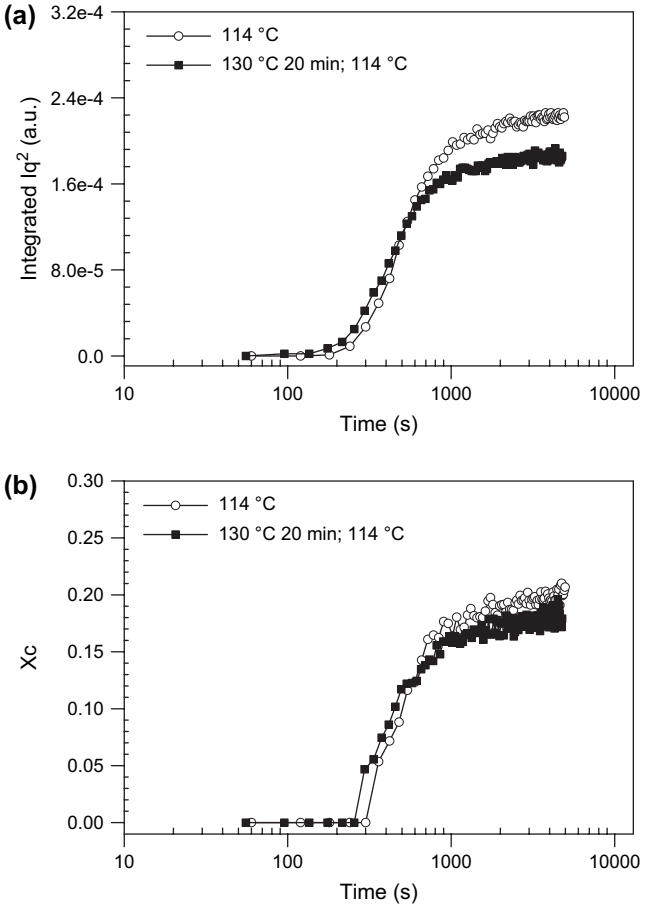

Fig. 5. Variations of (a) integrated Iq^2 of SAXS and (b) WAXD crystallinity, X_c, of the PEH/PEB 50/50 blend with time for the single quench and double quench procedures, respectively. Note that the relative standard deviations for Iq^2 in (a) and X_c in (b) are less than 1% and 3%, respectively.

quench and double quench procedures (two *S*-shape fitting curves were constructed to indicate the trends of the variations). In the initial stage of crystallization ($t_c \leq 140$ s), the integrated Iq^2 values in the two procedures are both near zero, indicating the absence of lamellar stacks during the initial induction period. After the induction period, the integrated Iq^2 values dramatically increase with time, whereas after about 1000 s they almost reach the plateau values and show only slight increase. The sharp increase of scattering intensity was due to the formation of stacking lamellae of PEH component in the blend. Fig. 5b illustrates the time evolution of crystallinity, X_c, in the single quench and double quench procedures. It is seen that the development of X_c also exhibits an *S*-shape like curve in the same manner as that in Fig. 5a. However, the induction period observed in the WAXD data is delayed compared with that observed in the SAXS data, which is probably due to the more sensitive detection limit of SAXS than WAXD [31]. Generally, the detection limits of crystallinity by SAXS (ca. 0.1%) and WAXD (ca. 1%) are different. Since the crystallinity in the early stage is quite low, the WAXD technique may not be able to detect it. On the contrary, the lower fraction of crystal phase can be readily detected by SAXS technique as long as the density contrast between constituting phases is sufficient and the length scale of periodicity is within the SAXS detecting range (i.e., less than 100 nm). In a previous publication, we noted that the integrated Iq^2 value from SAXS is proportional to crystallinity in the initial crystallization stages when the crystallinity is low [31].

Comparing the results from the single quench and double quench procedures (Fig. 5a and b), a common feature was found. In the early stages of crystallization, both values of integrated Iq^2 and X_c, are slightly higher in the double quench than those in the single quench. Thus, the induction period and the half time of crystallization must be shorter in the double quench than those in the single quench. It is interesting to note that both time-evolution curves for SAXS and WAXD crossover and eventually reverse in the late stages of crystallization. The crossover time for SAXS was about 500 s (Fig. 5a) and that for WAXD was about 600 s (Fig. 5b). The above findings indicate that when crystallization reaches the late stages, the integrated Iq^2 and X_c coherently become lower and crystallization is more retarded in the double quench than that in the single quench. This phenomenon will be discussed in the section later.

Fig. 6 shows time evolutions of l_1, l_2, and long period, L, determined from the analysis of the Lorentz-corrected SAXS profiles. Compared with the lamellar thicknesses estimated from the TEM observations (to be discussed later), the distance l_2 (about 71.4 Å) from SAXS seems to agree well with the lamellar thickness from TEM (about 71–72 Å). Thus, we assign l_1 as the averaged amorphous layer thickness and l_2 as the averaged lamellar thickness. We note that the thickness distribution of the lamellar stacks determined by SAXS analysis is about 30.0 Å and this distribution is consistent with the TEM results. We further note that the difference between the long period, L (200 Å in Fig. 6), and the one ($q_m \approx 0.0175$ Å^{-1}, $L_B = 360$ Å) from the Bragg's law can be understood as follows. In an earlier work by Santa Cruz et al. [24] the different possibilities to obtain morphological parameters from SAXS data were discussed. One of the main conclusions was that the values of l_1, l_2, and L obtained

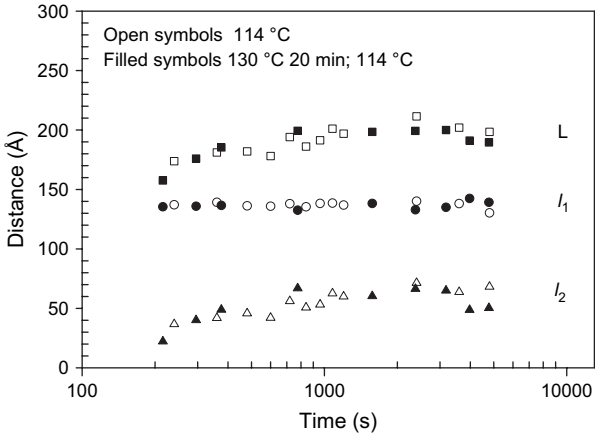

Fig. 6. Evolutions of long period L, lamellar thickness l_2 and amorphous layer thickness l_1 of the PEH/PEB 50/50 blend with time by simulations of the SAXS data for the single quench and double quench procedures.

after overlapping correction (i.e. from the simulated data) were the closest to the true morphological values, as in the case of this work when compared with the TEM results. Looking carefully at the TEM micrographs (in the latter section) one can readily see that branching at the end of the lamellar stack causes a broad distribution in the amorphous layer thickness, but not in the crystalline thickness, increasing the statistical distribution of the long period due to superposition effects. Superposition effects of the distribution functions can induce the shift of the peak in the reciprocal space rendering larger values of the long period obtained from Lorentz plots (L_B) and therefore producing large deviation with this type of calculation. Actually, the difference observed in this work is not so uncommon, since Santa Cruz et al. already showed that in some cases L_B can be almost double of that from the simulated data as seen in Fig. 7 of Ref. [24]. It is seen in Fig. 6 that there are no obvious differences between the morphological parameters of stacking lamellae determined from the single quench and double quench procedures. For both procedures, the lamellar thickness increases from ca. 30.0 Å to 71.4 Å during crystallization, while the amorphous thickness remains about constant. This is consistent with our previous results [14], where both lamellar thickness and long period increase with time due to the lamellar thickening mechanism at the relatively high crystallization temperature. This can be considered as an inherent consequence of chain-folding crystallization for flexible polymer molecules when the chains have sufficient mobility in the crystalline state to cause the crystal thickening. In addition, during crystallization the liquid–solid phase separation may occur and the amorphous PEB component would be possibly expelled out of the crystal growth front of PEH, which would consequently influence the crystal growth rate of PEH in the blend if compared with the neat PEH [14]. Although the almost identical morphological features in the two quench procedures indicate that the influences of LLPS on crystallization in these procedures are not reflected at the lamellar scale level, the effect of the earlier stage LLPS on crystallization mainly functions on the changes of crystallization kinetics, such as nucleation and growth rates.

3.2. DSC results

DSC scans were carried out using the same procedures as those employed in the SAXS/WAXD experiments. The original exotherms during isothermal crystallization of the PEH/PEB 50/50 blend, corresponding to the single quench and double quench procedures, are illustrated in Fig. 7a. The evolution curves of integrated heat flow for the single quench and double quench procedures are shown in Fig. 7b. It is seen that the integrated heat flow also exhibits an *S*-shape trend and the observed difference between the two quench procedures by DSC measurements shows an incredible accordance with that by X-rays (Fig. 5a and b). This observation suggests that different microscopic structures may form in the initial stage of crystallization under varying phase separation procedures, whereby the subsequent crystal growth can deviate from each other. Fig. 7c illustrates the results of the PEH/PEB 50/50 blend under isothermal crystallization temperature at 116 °C. It is noticed that the previously observed feature in time evolutions of integrated heat flow of the double quench and single quench also exists at 116 °C, although the feature seems to be weak. The reason for the weak feature may be that the temperature of 116 °C is closer to the crossover temperature of 118 °C than the temperature of 114 °C for the PEH/PEB 50/50 blend [12]. For further comparison, the same DSC procedures were also performed on pure PEH and the PEH/PEB 70/30 blend. In these two samples, the effects of LLPS on crystallization were expected to be absent or much less significant than that in the PEH/PEB 50/50 blend because of the lack of phase separation. This hypothesis was verified by results shown in Fig. 8a and b, where the two integrated heat flow curves during the different quench procedures are hardly discerned from each other. This indicates that, unlike the PEH/PEB 50/50 blend, the different quench procedures have almost no effects on the crystallization behaviors of pure PEH and the PEH/PEB 70/30 blend due to the absence of concentration fluctuations. In other words, the different crystallization behaviors in the single quench and double quench of the PEH/PEB 50/50 blend are indeed due to the effects of LLPS rather than being simply induced by different heat flow conditions.

3.3. Interplay between earlier stage liquid–liquid phase separation and crystallization

The process of spinodal decomposition is usually divided into three regimes [32,33]: (1) the initial or the early stage (the time evolution of concentration fluctuations can be described by Cahn's linearized theory [34]), where the wavelength of the fluctuations is invariant while the corresponding amplitude increases exponentially with time, (2) the intermediate stage, where both the wavelength and the amplitude of concentration fluctuations grow with time, and (3) the late stage, the amplitude of concentration fluctuations reaches an equilibrium value and the domain coarsening is only achieved by self-similarity in term of the scaling law. Many theoretical [35,36] and experimental [33] studies have been carried out to define and determine the initial time scale of spinodal decomposition. For example, de Gennes [35] described the growth of initial stage concentration fluctuations by local adjustment of each chain through removing the "kinks" in their tubes. In this case, the process of the local adjustment may be too rapid to be detected by general experimental techniques. According to Binder [36], for a polymer chain with $N \approx 3 \times 10^3$ and reorientation rate $W \approx 10^{10}$, the relaxation rate $\tau_{q_m}^{-1}$ (q_m is the wave-vector at which the growth rate of concentration fluctuations is maximum) is approximately 1 s^{-1}. Since for PEH and PEB, $N \approx 4 \times 10^3$ and 2×10^3, respectively, $\tau_{q_m}^{-1}$ of the blend should be roughly at the same time scale as that from Binder's calculation. Therefore, we consider that the conditions of 20 min LLPS at 130 °C in the double quench would be theoretically far beyond the initial stage of phase separation. Although there are no supporting light scattering data to describe the phase separation kinetics for PEH/PEB blends due to the nearly isorefractive indices between the two consisting

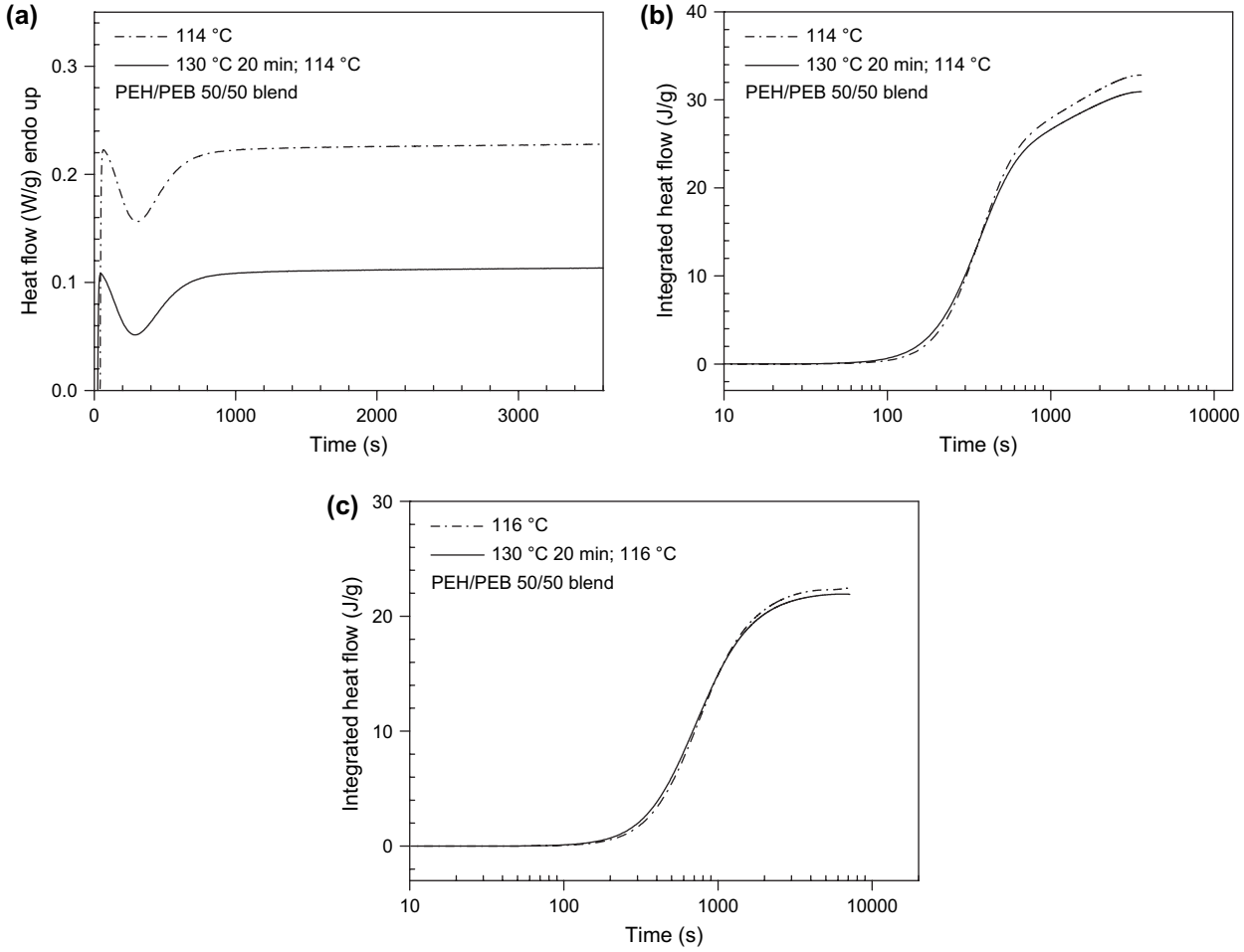

Fig. 7. (a) DSC exothermal curves for the PEH/PEB 50/50 blend during crystallization at 114 °C in the single quench and double quench procedures; (b) time evolution of integrated heat flow for the PEH/PEB 50/50 blend during crystallization at 114 °C and (c) that at 116 °C in the single quench and double quench procedures.

components, it can be basically determined that 20 min LLPS at 130 °C should be in the intermediate stage, where the interdiffusion induced concentration fluctuations and interfacial tension may co-exist, which can be judged from the combination of rheological and phase-contrast microscopy results [8,12,13] shown in Fig. A1 in Appendix. While in the single quench, LLPS and crystallization may simultaneously occur and the spinodal decomposition should be in the initial or early stage, which was also verified by Tanaka and Nishi [37,38].

It was shown that the crystallization rate at 114 °C was relatively fast because of the large supercooling depth in polyethylene [13]. Once crystallization begins, the process of LLPS would be ''locked in'' [9,10] and cannot further develop in either single quench or double quench procedure. The only differences between the two procedures are the initial nucleation process and the late stage crystal growth. In the single quench procedure, the simultaneously occurred spinodal decomposition can assist the crystal nucleation due to the decreased energy barrier [15,16]. In contrast, the situation is more complex in the double quench procedure. With 20 min of LLPS, the amplitude of concentration fluctuations could amplify and the domain coarsening might simultaneously begin [39]. As a result, a larger driving force for nucleation in double quench might be obtained than that in single quench (only the fluctuations with wavelengths larger than the critical value can induce nucleation for crystallization). Thus, the nucleation density and nucleation rate should be both higher in double quench than those in single quench, which has been also verified by Madbouly and Ougizawa [20]. This argument is consistent with the higher values of integrated Iq^2, X_c, and integrated heat flow in double quench than those in single quench in the early stage of crystallization (as shown in Figs. 5 (a and b) and 7 (b and c). In the late stage of crystallization, the morphological parameters for these two procedures crossover and the responses reverse. This can be explained as follows. In the single quench procedure, the simultaneously occurring LLPS was mostly frozen by crystallization and then the phase domain coarsening was not able to proceed. Thus, the growth of the lamellae could not be affected or suppressed by the phase domains with sharp phase boundaries. While in the double quench procedure (e.g. after 20 min of LLPS at 130 °C), the coarsening process began and the phase domains formed before crystallization (although this could not be clearly

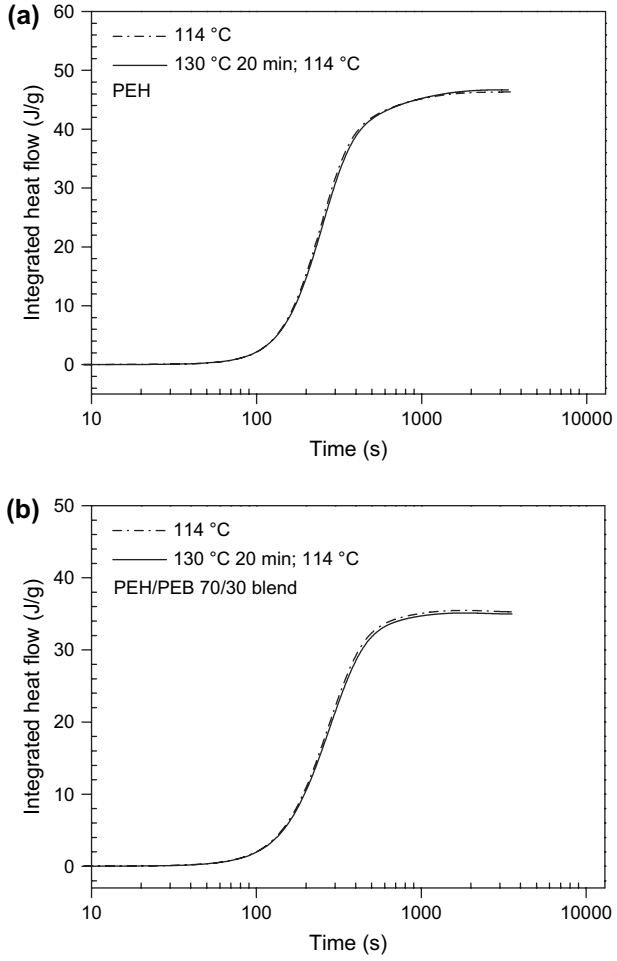

Fig. 8. Time evolution of integrated heat flow for (a) PEH and (b) the PEH/PEB 70/30 blend during crystallization at 114 °C in the single quench and double quench procedures.

detected by optical microscopy). As a result, the resulting phase domains were ''locked in'' and the subsequent crystallization possibly occurred mainly in the PEH-rich phase domains. In the late stage of crystallization, the trapped phase domains prevented the diffusion of PEH chains to the growth fronts of stacking lamellae from the PEB-rich phase domains [37,38]. As a result, the parameters of integrated Iq^2, X_c, and integrated heat flow (Figs. 5 (a and b) and 7 (b and c), respectively) became lower in the double quench procedure than those in the single quench procedure. Based on the above argument, through the intentionally controlled LLPS with a time period of 20 min in the double quench procedure, the crystallization rate in the early stage appeared to be accelerated, while that in the late stage appeared to be retarded. Thus, the LLPS could possess opposite effects on the crystallization behavior, depending on the time scales of these two different pathways.

3.4. Morphology observed by TEM

Fig. 9 shows TEM micrographs of the PEH/PEB 50/50 blend at different scales for the single quench (labeled by ''A'') and double quench (labeled by ''B'') procedures at isothermal crystallization temperature of 114 °C. The samples used for TEM observations were extracted from the samples used after the X-ray scattering measurements. In Fig. 9a, it seems that the clusters of lamellae are relatively larger and the stacking lamellae look longer in micrograph A than those in micrograph B. This indicates that in the single quench procedure, the crystal lamellae can develop freely without obvious interference of the phase-separated domains. In the double quench procedure, the growth of crystal lamellae seems to face difficulty to pass through the PEB-rich domains, such that the lamellar stacks piled in a more isolated and disordered manner. It has been reported that the small, dispersed and imperfect crystals could be generated from the PEB-rich phase domains because the concentration of PEH in the PEB-rich phase domains might be still high after 20 min of LLPS in the double quench procedure [17]. In order to obtain the structure information of stacking lamellae in more detail, the magnified micrographs are shown in Fig. 9b. It is seen that the lateral size of lamellar stacks in micrograph A is about twice of that in micrograph B. In addition, the lamellar stacks in micrograph A exhibit the feathers-like texture, while that in micrograph B exhibit the short fluffs-like texture. Fig. 9c indicates that there is no obvious difference of lamellar thickness between micrographs A and B. The above findings suggest that the crystal lamellar morphology developed in the late stage of crystallization is more regular and denser in single quench than in double quench, which is also consistent with the results from Figs. 5 (a and b) and 7 (b and c). Fig. 9d illustrates the comparison of the lamellar thickness distributions from the two quench procedures estimated by TEM observations. The estimated lamellar thickness range is between 72 and 101 Å for single quench and 71 and 92 Å for double quench. It should be noted here that when microtoming the randomly oriented samples, the cutting just cannot always be perpendicular to the lamellar surface. If the cutting is tilted, the observed crystalline lamellar (those unstained white layers in TEM micrographs) thickness should be larger than the actual thickness of a crystalline lamella. To obtain the accurate thickness for the crystalline lamellae, the smallest thickness for a large number of observed crystalline lamellae should be close to the actual crystalline lamellar thickness. From the data shown in Fig. 9d, the smallest thickness for single-quenched sample is ca. 72 Å and that for double-quenched sample is ca. 71 Å. These two values are close to the calculated crystalline lamellar thicknesses of 71.4 Å in Fig. 6 by using the correlation function analysis. In addition, the slightly narrower lamellar thickness distribution in double quench is also consistent with our recent observation that the long period distribution became narrowed with LLPS time [18]. In that study, the narrower long period distribution was explained by the reduced amorphous gap. However, from the results in this study, it may also be attributed to the variations of lamellar thickness distribution. Although there was no distinct difference of the average lamellar thickness between the two procedures in Fig. 9d, the area below the fitted curve in single quench was relatively larger than that in double quench. This observation is also consistent with the variations of the crystallinity, X_c, during the late stage of crystallization (Fig. 5b). In

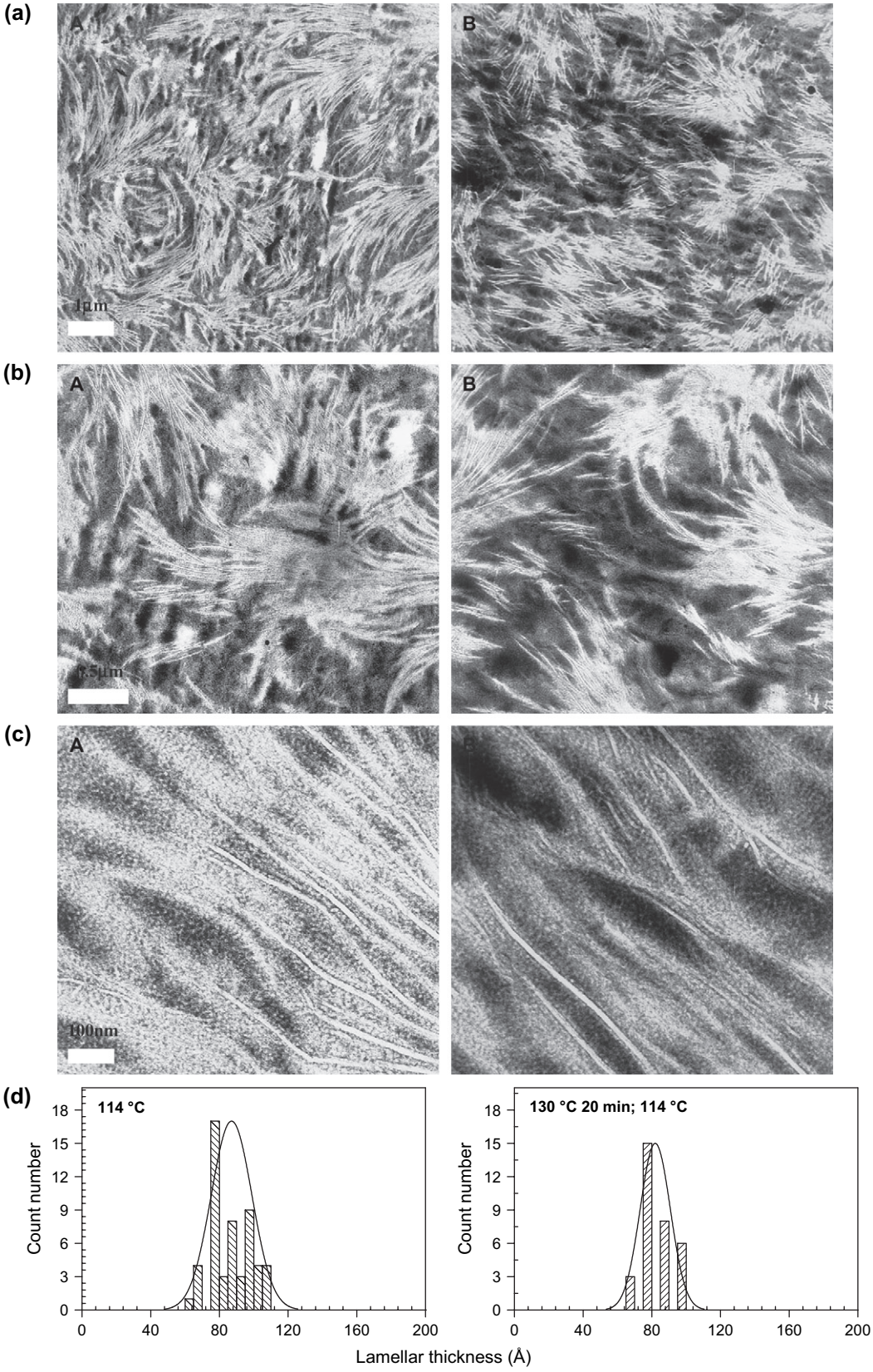

Fig. 9. (a, b, c) TEM micrographs of the PEH/PEB 50/50 blend isothermally crystallized at 114 °C for the single quench (labeled "A") and double quench (labeled "B") procedures at different magnifications; and (d) the count numbers of lamellae and the corresponding fitted curves as functions of lamellar thickness for the single quench and double quench procedures, respectively.

summary, the LLPS with short time exhibited little effects on the scale of lamellar thickness, but notable effects on the structures of larger scales such as lamellar stack sizes and the corresponding size distributions.

4. Conclusions

In this study, the interplay between the early and intermediate stage liquid–liquid phase separation (LLPS) and crystallization of the PEH/PEB 50/50 blend were studied by time-resolved simultaneous SAXS/WAXD, DSC and ex situ TEM measurements. It was found that in the single quench procedure, the LLPS and crystallization could simultaneously occur and the initial stage of concentration fluctuations would assist the nucleation process in crystallization. In the double quench procedure, the concentration fluctuations of LLPS were enhanced, and the phase domains were gradually formed after 20 min of annealing at 130 °C. As a result, the enhanced concentration fluctuations could greatly facilitate the nucleation process for crystallization. And hence, the values of integrated Iq^2 and crystallinity X_c were consistently higher in double quench than those in single quench during the early stage of crystallization. In the late stage of crystallization, these parameters crossed over and then reversed, which was due to the lamellar growth suppression affected by the presence of phase domains in double quench. This finding was further confirmed by DSC measurements. The lamellar thickness determined by simulation of the SAXS data exhibited a good accordance with that observed by TEM. Both SAXS and TEM results indicated that the earlier stage LLPS prior to crystallization could affect the resulting lamellar structures of the PEH/PEB blends, such as the sizes of lamellar stacks and the lamellar stack distributions. In contrast, the averaged lamellar thickness and the long period at a relatively smaller scale did not show any obvious difference between the two quench procedures.

Acknowledgements

Z.G. Wang thanks financial supports from ‘‘One Hundred Young Talents’’ Program of Chinese Academy of Sciences, National Science Foundation of China with Grant No. 10590355 for the Key Project on Evolution of Structure and Morphology during Polymer Processing and National Science Foundation of China with Grant No. 20674092 and 50573088. H. Wang acknowledges the support by the National Science Foundation under Grant No. 0348895. B.S. Hsiao acknowledges the financial support from the National Science Foundation (DMR-0405432).

Appendix

Fig. A1 depicts the combination of rheological and phase-contrast optical microscopy results for PEH/PEB 50/50 blend at 130 °C. It can be seen from the rheological time sweep curve, in the very initial stage, the storage modulus G' sharply increases with time and reaches a maximum at time less than

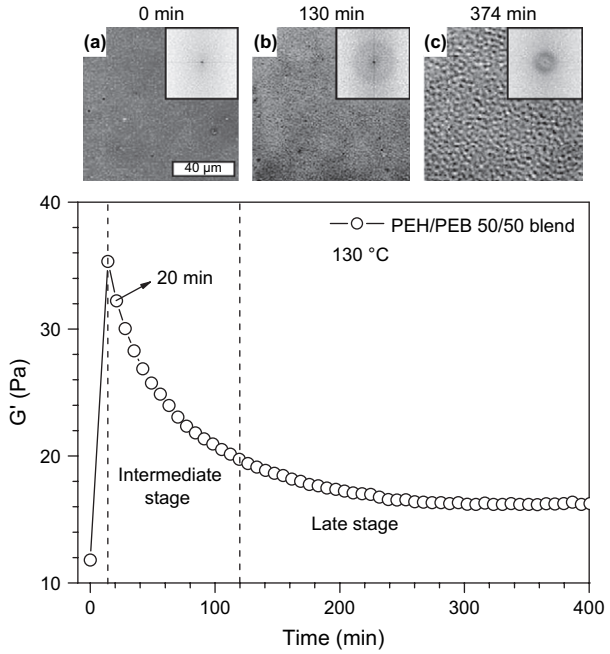

Fig. A1. Evolution of storage modulus, G', during time sweep for PEH/PEB 50/50 blend at 130 °C with a fixed frequency of 0.03 rad/s and strain of 5% [8]. The corresponding phase-contrast optical micrographs on the top show the isothermally phase-separated morphologies and 2D-FFT images at 130 °C for different annealing time of (a) 0 min, (b) 130 min, (c) 374 min [13]. The scale bar in (a) represents 40 μm.

14 min because of the exponentially increased amplitude of concentration fluctuations. In the intermediate stage, the simultaneously increased concentration fluctuations and wavelength lead to the dramatic decreasing of G'. In the late stage, the concentration fluctuations basically reach equilibrium and the interfacial tension becomes dominant, which result in continuous and slow decreasing of G' with the increasing phase domains. According to the phase-contrast optical micrographs in Fig. A1, the phase domains can hardly be detected before 130 min, but many small clusters form at this stage; obvious phase domains can be observed and self-similarity occurs after 130 min, which is regarded as the typical character of the late stage spinodal decomposition. Therefore, we consider that the time range from 14 min to 130 min should belong to the intermediate stage. Thus, the instant of 20 min marked in Fig. A1 should belong to the intermediate stage of phase separation.

References

[1] Crist B, Hill MJ. J Polym Sci Part B Polym Phys 1997;35:2329.
[2] Hill MJ, Morgan RL, Barham PJ. Polymer 1997;38:3003.
[3] Hill MJ, Barham PJ. Polymer 2000;41:1621.
[4] Alamo RG, Graessley WW, Krishnamoorti R, Lohse DJ, Londono JD, Mandelkern L, et al. Macromolecules 1997;30:561.
[5] Wignall GD, Alamo RG, Londono JD, Mandelkern L, Kim MH, Lin JS, et al. Macromolecules 2000;33:551.
[6] Crist B, Nesarikar AR. Macromolecules 1995;28:890.
[7] Wang H, Shimizu K, Hobbie EK, Wang ZG, Carson Meredith J, Karim A, et al. Macromolecules 2002;35:1072.
[8] Niu YH, Wang ZG. Macromolecules 2006;39:4175.
[9] Inaba N, Sato K, Suzuki S, Hashimoto T. Macromolecules 1986;19:1690.

[10] Inaba N, Yamada T, Suzuki S, Hashimoto T. Macromolecules 1988;21:407.
[11] Cham PM, Lee TH, Marand H. Macromolecules 1994;27:4263.
[12] Wang H, Shimizu K, Kim H, Hobbie EK, Wang ZG, Han CC. J Chem Phys 2002;116:7311.
[13] Shimizu K, Wang H, Wang ZG, Matsuba G, Kim H, Han CC. Polymer 2004;45:7061.
[14] Wang ZG, Wang H, Shimizu K, Dong JY, Hsiao BS, Han CC. Polymer 2005;46:2675.
[15] Zhang XH, Wang ZG, Muthukumar M, Han CC. Macromol Rapid Commun 2005;26:1285.
[16] Zhang XH, Wang ZG, Dong X, Wang DJ, Han CC. J Chem Phys 2006;125:024907.
[17] Zhang XH, Wang ZG, Han CC. Macromolecules 2006;39:7441.
[18] Zhang XH, Wang ZG, Zhang RY, Han CC. Macromolecules 2006;39:9285.
[19] Tsuburaya M, Saito H. Polymer 2004;45:1027.
[20] Madbouly SA, Ougizawa T. Macromol Chem Phys 2004;205:1923.
[21] Matsuba G, Shimizu K, Wang H, Wang ZG, Han CC. Polymer 2003;44:7459.
[22] Matsuba G, Shimizu K, Wang H, Wang ZG, Han CC. Polymer 2004;45:5137.
[23] Song HH, Wu DQ, Chu B, Satkowski M, Stein RS, Phillips JC. Macromolecules 1990;23:2380.
[24] Santa Cruz C, Stribeck N, Zachmann HG, Balta Calleja FJ. Macromolecules 1991;24:5980.
[25] Debye P, Anderson Jr HR, Brumberger H. J Appl Phys 1957;28:679.
[26] Porod G. Kolloid ZZ Polym 1951;24:83;
Porod G. Kolloid ZZ Polym 1952;125:51.
[27] Ruland W. J Appl Crystallogr 1971;4:70.
[28] Fiedel HW, Wenig W. Colloid Polym Sci 1989;267:389.
[29] Ruland W. Colloid Polym Sci 1977;255:417.
[30] Stribeck N, Ruland W. J Appl Crystallogr 1978;11:535.
[31] Wang ZG, Hsiao BS, Sirota EB, Agarwal P, Srinivas S. Macromolecules 2000;33:978.
[32] Hashimoto T, Itakura M, Hasegawa H. J Chem Phys 1986;85:6118.
[33] Hashimoto T, Itakura M, Shimidzu N. J Chem Phys 1986;85:6773.
[34] Cahn JW. J Chem Phys 1965;42:93.
[35] de Gennes PG. J Chem Phys 1980;72:4756.
[36] Binder K. J Chem Phys 1983;79:6387.
[37] Tanaka H, Nishi T. Phys Rev Lett 1985;55:1102.
[38] Tanaka H, Nishi T. Phys Rev A 1989;39:783.
[39] Rappl TJ, Balsara NP. J Chem Phys 2005;122:214903.